Epitaxial Ultrathin Hi-K AlBN/GaN FerroHEMTs

C. Savant[1†], K. Nomoto[2†], T. Nguyen[1], W. Zhao[3], S. D. Funni[1], S. Ma[1], M. Ramesh[2], J. J. Cha[1], H. Xing[1,2,4], D. Jena[1,2,4]
[1]Department of Materials Science and Engineering, Cornell University, Ithaca, NY 14853, USA,
[2]School of Electrical and Computer Engineering, Cornell University, Ithaca, NY 14853, USA,
[3]School of Applied and Engineering Physics, Cornell University, Ithaca, NY 14853, USA,
[4]Kavli Institute at Cornell for Nanoscale Science, Cornell University, Ithaca, NY 14853, USA
[†]Equal Contribution. Email: cps259@cornell.edu, kn383@cornell.edu

2025 IEEE International Electron Devices Meeting (IEDM) | 979-8-3315-6785-9/25/$31.00 ©2025 IEEE | DOI: 10.1109/IEDM50572.2025.11353577

***Abstract*—We report the first observation of ferroelectric gating in ultrawide bandgap, high-K, crystalline AlBN barrier GaN high electron mobility transistors (FerroHEMTs) using the thinnest ferroelectric nitride barrier to date. We observe a strong effect of gate length scaling from L_g = 1.5 μm to 44 nm on the ferroelectric gating performance of AlBN/GaN FerroHEMTs. While the short L_g = 44 nm gate length devices exhibit ferroelectric gating with large repeatable hysteretic I_d - V_{gs} loops and 40 mV/decade sub-Boltzmann characteristic, the devices with longer L_g = 800 nm to 1.5 μm exhibit little to no hysteresis. We report the first RF performance of AlBN/GaN HEMTs with f_T/f_{MAX} = 76/139 GHz, introducing first epitaxial ultrawide bandgap, high-K, and ferroelectric AlBN barrier technology to RF and mm-wave electronics.**

I. Introduction

Today's state-of-the-art GaN HEMT RF power amplifiers are nearing their performance limits due to the modest dielectric constant and bandgap of conventional AlGaN and AlInN heterostructure barriers. [1] The recent discovery of ferroelectricity [2] and high-K [3] in epitaxial AlScN barriers has introduced a promising new path forward similar to the case of HfO_2 for Silicon FETs. A new class of FerroHEMT devices using 90 nm T-gate technology was realized. [4] The decrease in bandgap and increase in susceptibility to chemical oxidation as the Sc content is increased in AlScN places limitations on this barrier material. Furthermore, the effect of gate length scaling on FerroHEMTs remains unexplored.

Fig. 1(a) shows that compared to AlGaN, AlInN, and AlScN barriers, an AlBN barrier maintains an ultrawide bandgap (UWBG) energy near 6.0 eV for high breakdown voltage. Fig. 1(b) shows that in addition, AlBN exhibits a higher dielectric constant than AlScN of corresponding bandgap [1], [5]. Fig. 1(c) shows how scaling is enabled by boosting the polarization-induced 2D electron gas (2DEG) charge density using an AlBN barrier on GaN compared to state-of-the-art AlGaN, AlInN, and AlScN barrier layers. A 7% B-containing epitaxial AlBN layer increases the strain-limited critical thickness of AlN by 50% with hi-K barrier properties on GaN [1].

While epitaxial AlBN offers a compelling new UWBG epitaxial hi-K barrier opportunity for GaN RF and mm-wave transistors [1], and ferroelectic switching of metal-AlBN-metal (MFM) has been observed in epitaxial AlBN thin films, the AlBN barrier FerroHEMTs have not been realized yet.

We report the first observation of ferroelectric gating in ultrathin epitaxial AlBN barrier GaN FerroHEMTs. We observe that ferroelectric gating is strongly dependent on L_g: shortest L_g devices exhibit strong ferroelectric gating, while ferroelectricity does not manifest for long L_g devices. The short L_g FerroHEMTs exhibit sub-Boltzman characteristics and small signal speeds of f_T/f_{MAX} =76/139 GHz.

II. Epitaxial Growth

Fig. 2(a) shows a MFM capacitor structure comprising 50 nm β-Nb_2N bottom electrode layer and 150-250 nm AlBN layers with 0-18% B epitaxially grown by MBE, followed by evaporated Ni/Au top electrode. Fig. 2(b) shows the relative dielectric permittivity, ϵ_r, extracted from C-V measurements at 0 V, 300 K. While the control AlN exhibits a relative permittivity ϵ_r^{AlN} = 8.8, the AlBN films with 5%, 18% B exhibit high ϵ_r^{AlBN} = 15.6, 17 at 400 kHz. Frequency dependence indicates small space-charge polarization effects for AlN, $Al_{0.95}B_{0.05}N$ films. Thus, AlBN films exhibit a higher ϵ_r than Al(Sc/In/Ga)N alternatives as indicated in Fig. 2(c) and Fig. 1(b). The polarization-electric field (P-E) loops extracted from the positive-up-negative-down (PUND) measurement in Fig. 2(d) indicate ferroelectricity in the epitaxial AlBN films.

Fig. 3(a) shows an AlBN/GaN HEMT layer structure with 7% B measured by X-ray photoelectron spectroscopy (XPS), which was epitaxially grown by MBE directly on semi-insulating 6H-SiC substrates with a 120 nm AlN nucleation layer and a 600 nm unintentionally doped (UID) GaN buffer layer. The corresponding energy band diagram calculated using self-consistent Schrödinger Poisson solution in Fig. 3(b) indicates a 2DEG channel at the AlBN/GaN heterojunction shown by $|\Psi_1|^2$. Fig. 3(c) shows an AFM micrograph, and Fig. 3(d) shows a streaky RHEED pattern showing 0.56 nm rms roughness of the wurtzite AlBN/GaN surface. Scanning transmission electron microscopy (STEM) images in Fig. 3(e) confirm an as-grown metal-polar, crystalline, ultrathin 4 nm AlBN barrier with 1 nm GaN cap on UID GaN buffer.

III. Device design and fabrication

Figs. 4(a,b) shows the process flow with regrown n^+GaN ohmic contacts and a schematic cross-section for realizing

AlBN/GaN HEMTs using 2DEG at the AlBN/GaN heterojunction as the conducting channel. We used a SiO_2/Cr hard mask to define the source/drain regions. To form ohmic contacts to 2DEGs, lithographically defined ICP etching and regrowth of heavily Si-doped n^+GaN ($N_d \sim 10^{20}$/cm^3) was performed by MBE. Ti/Au source/drain was deposited on the n^+GaN, and Ni/Au was deposited as gate metal. We combined optical and electron beam lithography (EBL) processes to realize 44 nm $\leq L_g \leq$ 1500 nm. Fig. 4(c) shows a SEM top-view image of the final AlBN/GaN HEMT with source, drain, and gate metal pads. The SEM inset shows a scaled T-gate device with $L_g \approx$ 44 nm. Fig. 4(d) shows the contact resistances between metal-regrown n^+GaN (low, R_c = 0.05 Ω·mm) and 2DEG-n^+GaN (moderate, R_c = 0.2 Ω·mm) extracted from transfer length method (TLM) structures in Fig. 4(e).

IV. Results and Discussion

Fig. 5(a) compares the effect of device fabrication on the 300 K Hall effect transport properties of the 2DEG channel. The as-grown sample exhibited 2DEG sheet carrier density $N_s \sim 1.04\times10^{13}$/cm^2, electron mobility $\mu \sim$ 461 cm^2/V.s, and sheet resistance R_{sh} = 1297 Ω/sq. After HEMT processing, the Hall effect data of processed Van der Pauw patterns with regrown n^+GaN contacts are seen to degrade the sheet resistance due to lowering of the 2DEG density, and similar or lower mobilities than the as-grown values.

Fig. 5(b) shows the structure used for capacitance-voltage (C-V) measurements on metal-insulator-semiconductor (MIS) capacitors with 2DEG channel accessed using regrown n^+GaN as bottom electrode and 20 μm diameter circular Ni/Au top electrode. Fig. 5(c) shows the measured C-V data (dots) fitted to a Schrödinger-Poisson C-V simulation (solid line). This figure indicates a near doubling of the dielectric constant of ϵ_r^{AlBN} = 16.2 for the $Al_{0.93}B_{0.07}N$ barrier compared to ϵ_r^{AlN} = 8.8 for AlN.

Fig. 6(a) shows the output characteristics of a $L_g \approx$ 44 nm, L_{sd} = 600 nm and W_g = 50 μm AlBN/GaN HEMT, and Fig. 6(b) and (c) show the transfer curves of this device in log and linear scales respectively. An on-current of 580 mA/mm with an on-resistance of R_{on} = 3.41 Ω·mm at V_{gs} = 2 V and R_{on} = 9.5 Ω·mm at V_{gs} = 0 V was observed. An on/off ratio of 10^7 limited by gate leakage, with a threshold voltage of ∼ -0.8 V to -0.12 V with on→off and off→on sweeps was observed. Fig. 6(d) shows a peak transconductance of g_m ∼272 mS/mm.

The transfer curves in Fig. 6(b) exhibit large counterclockwise (CCW) hysteresis loops translating to the linear scale hysteretic drain current seen in Fig. 6(c). At $V_{ds} = 1$ V, a steep sub-Boltzmann slope of 40.5 mV/decade is observed for the off→on voltage sweep, and a subthreshold swing (SS) of 73.2 mV/decade is observed for the on→off voltage sweep. The hysteresis window of gate voltage ΔV_g^{hys} is 3.1 to 3.9 V. Large repeatable counterclockwise hysteresis with sub-Boltzmann characteristics indicates ferroelectric gating [4] in AlBN FerroHEMTs. Based on the $t = 4$ nm AlBN barrier thickness, the hysteresis window of $2|E_c|t \sim$ 3.5 V is consistent with $|E_c|$ ∼4.375 MV/cm.

Fig. 7(a-c) shows how the transfer curves of AlBN/GaN HEMTs evolve for $L_g = 44 \rightarrow 800 \rightarrow 1500$ nm, with corresponding scaled L_{sd} for W_g = 50 μm. Several devices measured for the shortest $L_g \approx 44$ nm repeatably show counterclockwise hysteresis in the transfer curves with sub-Boltzman SS. While this FerroHEMT behavior is seen for $L_g \approx$ 44 nm devices, those with larger L_g do not exhibit hysteretic characteristics, as seen in Fig. 7(b) and (c). Figs. 7(d) and (e) show the hysteresis window plotted as a function of L_g and L_{sd}, indicating that device scaling has a strong effect on ferroelectric gating potentially indicating a measure of ferroelectric domain sizes.

Fig. 8(a) shows the small-signal RF characteristics of the L_g =44 nm AlBN/GaN HEMT. A -20 dB/dec extrapolation yields cutoff frequencies of f_T/f_{MAX} = 76/139 GHz. This is the first report of RF characteristics of AlBN barrier HEMTs. Fig. 8(b) shows the equivalent small signal circuit model obtained using a standard extraction procedure [6] and the extracted circuit elements of the HEMT. The extracted RF parameters are $g_m^{ext} = 120$ mS/mm (smaller than DC), $R_{ds} =$ 1020 Ω and $C_{gd} = 1$ fF. The simulated f_T/f_{MAX} of 76/138 GHz closely matches the measured values of 76/139 GHz of the AlBN barrier HEMTs.

V. Conclusions and Future Work

This work shows the high potential of AlBN barrier GaN HEMTs compared to existing AlGaN, AlScN barriers benchmarked in Fig. 8(d). Short L_g AlBN/GaN FerroHEMTs reported here with large hysteresis and sub-Boltzman characteristic have the thinnest epitaxial ferroelectric nitride barriers reported to date. Gate length scaling enables single chip integration of FerroHEMT devices with large hysteresis and HEMT devices with negligible hysteresis. While we introduce the first epitaxial ultrawide bandgap AlBN barrier technology to RF and mm-wave electronics, achievable 3× improvement in 2DEG mobility, low-resistance regrown contacts, and device passivation will improve the performance dramatically. The UWBG, high-K properties of AlBN will increase the breakdown voltage in FerroHEMTs by reducing the gate leakage, while the high thermal, chemical, and radiation tolerance of AlBN will enable GaN HEMTs for use in harsh environments.

Acknowledgment

This work was supported by the SRC and DARPA through the Joint University Microelectronics Program (JUMP) 2.0 and performed at the Cornell NanoScale Facility, an NNCI member supported by NSF Grant No. NNCI-2025233.

References

[1] C. Savant *et al.*, *Appl. Phys. Lett.*, vol. 126, p. 112906, 2025.
[2] S. Fichtner *et al.*, *J. Appl. Phys.*, vol. 125, p. 114103, 2019.
[3] J. Casamento *et al.*, *Appl. Phys. Lett.*, vol. 120, p. 152901, 2022.
[4] J. Casamento *et al.*, in *2022 International Electron Devices Meeting (IEDM)*, 2022, pp. 11.1.1–11.1.4.
[5] J. Hayden *et al.*, *Phys. Rev. Mat.*, vol. 5, p. 044412, 2021.
[6] G. Dambrine *et al.*, *IEEE Transactions on Microwave Theory and Techniques*, vol. 36, no. 7, pp. 1151–1159, 1988.
[7] T. Nguyen *et al.*, in *2024 International Electron Devices Meeting (IEDM)*, 2024, pp. 9.5.1–9.5.4.

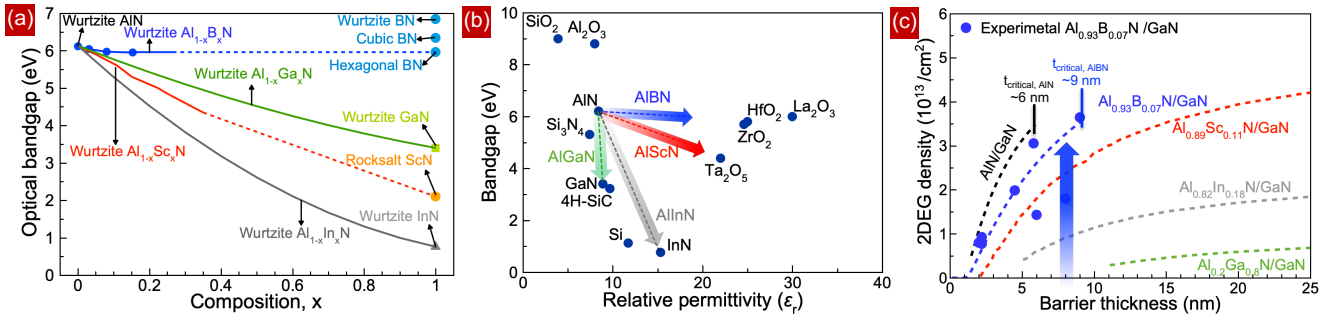

Fig. 1. AlBN is a promising barrier for GaN HEMTs because of (a) its ultrawide bandgap with (b) high dielectric constant and (c) high polarization-induced 2DEG density at AlBN/GaN heterojunctions compared to AlGaN/GaN, AlInN/GaN and AlScN/GaN heterojunctions. [7]

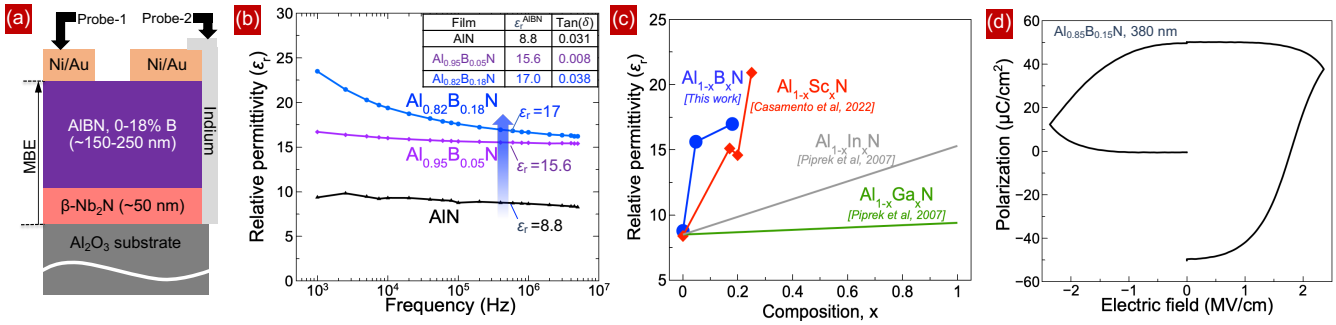

Fig. 2. (a) Heterostructure of MFM capacitors with epitaxial AlBN films used for C-V and PUND measurements. (b) Extracted relative dielectric permittivity, ϵ_r, at multiple measurement frequencies, indicating high-K of AlBN film compared to AlN with small space charge polarization. (c) Relative permittivity, ϵ_r, of Al(B/Sc/In/Ga)N films, showing high ϵ_r of AlBN films. (d) Measured ferroelectric P-E loops observed for Au/Ni/AlBN/β-Nb_2N heterostructure.

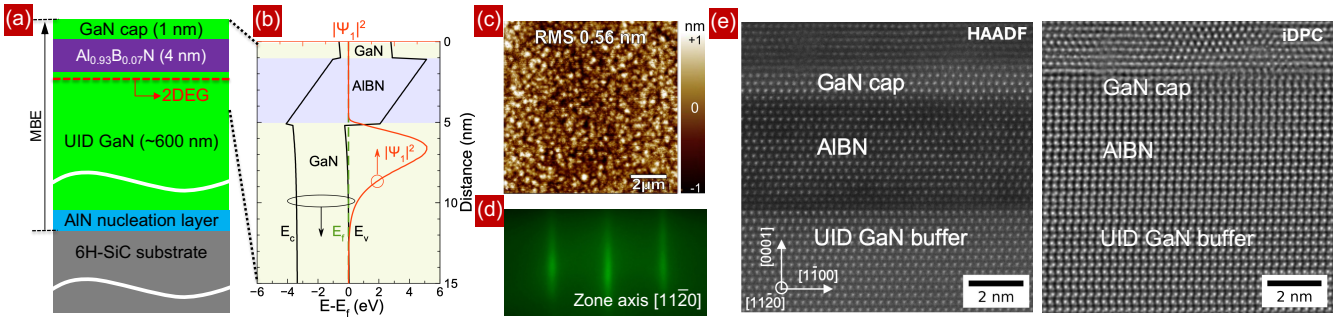

Fig. 3. (a) AlBN/GaN HEMT heterostructure, and (b) Energy band diagram indicating 2DEG at AlBN/GaN heterojunction, (c) AFM micrograph, and (d) RHEED pattern showing as-grown surface morphology of the wurtzite AlBN/GaN structure grown by MBE. (e) High-angle annular dark field (HAADF) and (f) Integrated differential phase contrast (iDPC) scanning transmission electron microscopy (STEM) images of ultrathin AlBN/GaN heterostructure.

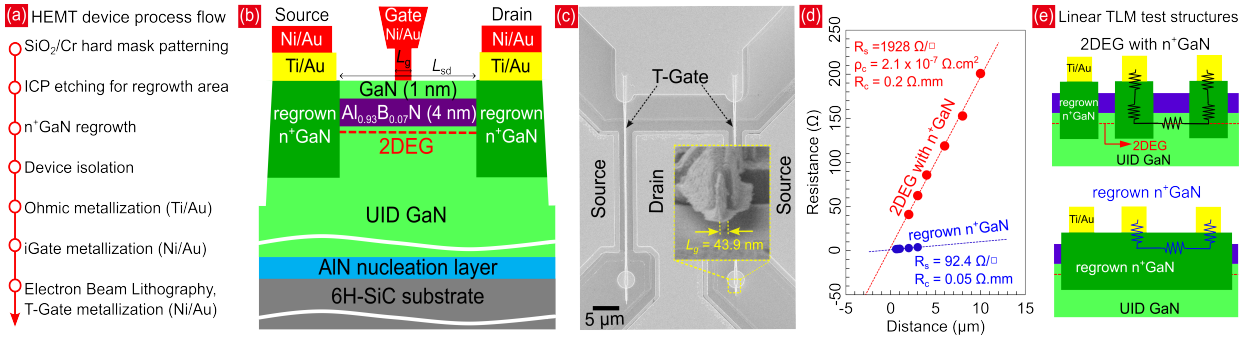

Fig. 4. (a) The device process flow of AlBN/GaN HEMTs with MBE regrown n^+GaN contacts. (b) Cross-section schematic of 4 nm AlBN barrier GaN FerroHEMT. (c) The SEM image of a processed FerroHEMT. The SEM inset shows an EBL T-gate with a gate width L_g = 44 nm. (d), (e) Ultralow contact resistances for the AlBN barrier FerroHEMT between the metal and the regrown n^+GaN regions and the n^+GaN regions and 2DEGs.

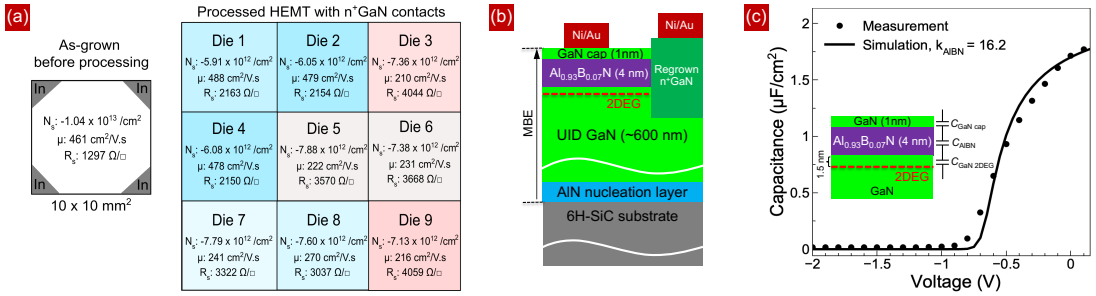

Fig. 5. (a) Hall effect measurements with Van der Pauw pattern showing the transport properties before- and after-fabrication across device dies. (b) MIS diodes used for C-V measurements, and (c) C-V of circular gate MIS diode in circles. Solid line is a model with dielectric constant $\epsilon_r^{\mathrm{AlBN}} \sim 16.2$.

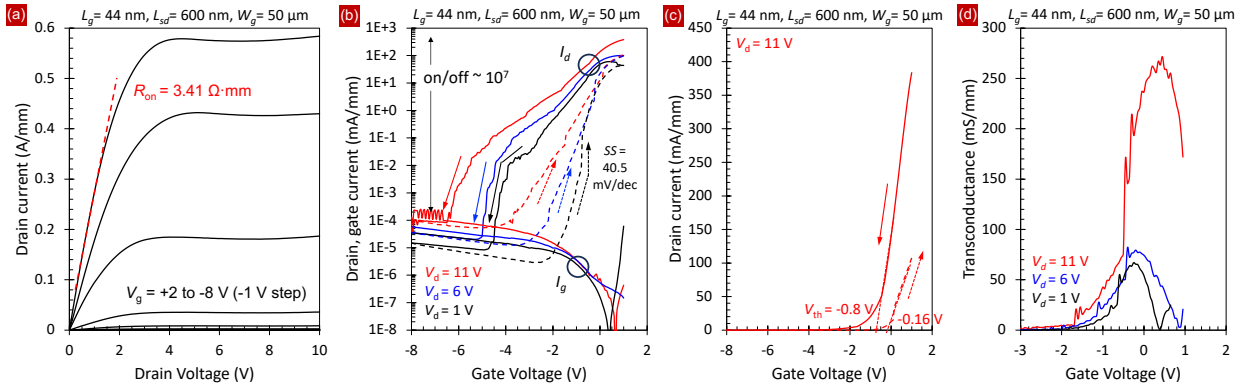

Fig. 6. Measured characteristics of ultrathin AlBN barrier FerroHEMT with L_g = 44 nm : (a) Output characteristics (b) Transfer characteristics in log scale, (c) linear scale, showing hysteresis, and (d) Transconductance $g_{m,ext}$ vs. V_{gs}. Repeatable counterclockwise hysteresis was observed in transfer curves.

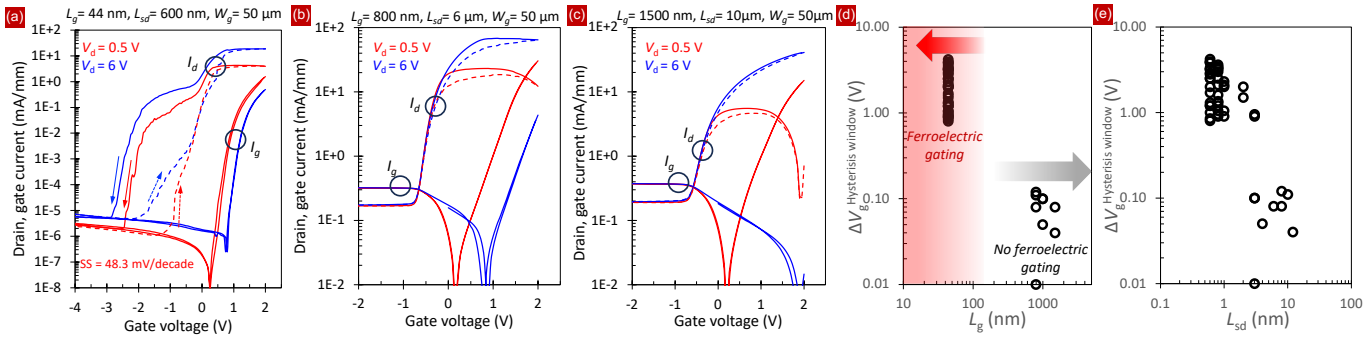

Fig. 7. (a) Measured transfer characteristics of AlBN HEMT with L_g = 44 nm (b) L_g = 800 nm and (c) L_g = 1500 nm. (d) Hysteresis window, V_{gs} as a function of gate length L_g and (e) source-drain distance L_{sd}.

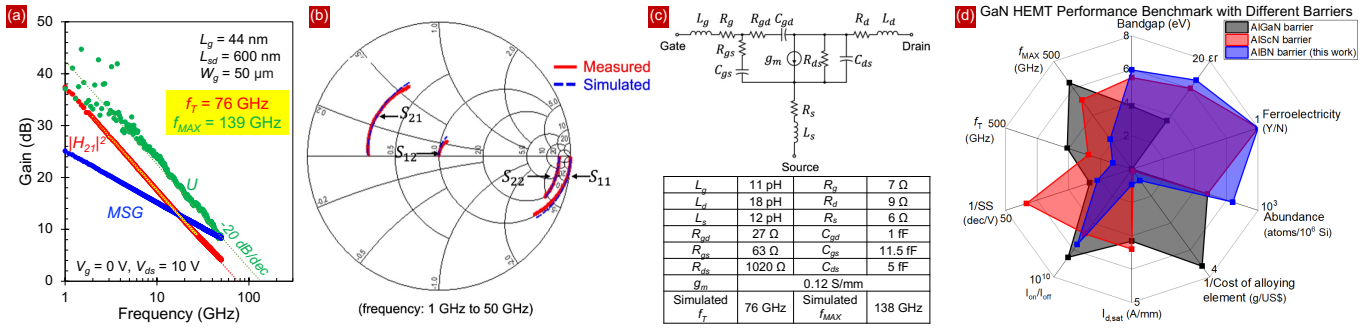

Fig. 8. (a) Measured cutoff frequencies of AlBN FerroHEMT showing f_T/f_{MAX} = of 76/139 GHz. (b) Comparison between measured and simulated S parameters. (c) Small signal equivalent circuit elements under V_g = 0 V, V_{ds} = 10 V. (d) GaN HEMT performance benchmark with different barriers.